Special Issue

En Face Spectral-Domain Optical Coherence Tomography for the Monitoring of Lesion Area Progression in Stargardt Disease

Paolo Melillo,[1] Francesco Testa,[1] Settimio Rossi,[1] Valentina Di Iorio,[1] Ada Orrico,[1] Alberto Auricchio,[2,3] and Francesca Simonelli[1]

[1]Eye Clinic, Multidisciplinary Department of Medical, Surgical and Dental Sciences, Second University of Naples, Naples, Italy
[2]Telethon Institute of Genetics and Medicine (TIGEM), Pozzuoli, Italy
[3]Department of Translational Medicine, "Federico II" University, Napoli, Italy

Correspondence: Francesca Simonelli, Eye Clinic, Multidisciplinary Department of Medical, Surgical and Dental Sciences, Second University of Naples, Via Sergio Pansini, 5, 80131 Naples, Italy; francesca.simonelli@unina2.it.

PM and FT contributed equally to the work presented here and should therefore be regarded as equivalent authors.

Submitted: November 26, 2015
Accepted: April 10, 2016

Citation: Melillo P, Testa F, Rossi S, et al. En face spectral-domain optical coherence tomography for the monitoring of lesion area progression in Stargardt disease. *Invest Ophthalmol Vis Sci*. 2016;57:OCT247–OCT252. DOI:10.1167/iovs.15-18751

Purpose. We investigated the progression of Stargardt disease (STGD1) over a multiyear follow-up by evaluating the macular lesion area as computed by an automatic algorithm from spectral-domain optical coherence tomography (SD-OCT).

Methods. We reviewed medical records of STGD1 patients, with a clinical and molecular diagnosis of STGD1 at a single institution, who underwent best-corrected visual acuity (BCVA), fundus photography, SD-OCT, full-field electroretinography, and, when available, fundus autofluorescence (FAF). Regression models were fitted on the selected clinical parameters; in particular, on the macular lesion area computed by SD-OCT, to evaluate the disease progression over a multiyear follow-up.

Results. The comparison between SD-OCT and FAF, available for 22 patients, showed that macular lesion area, assessed by SD-OCT, significantly correlated with the area of absent FAF ($P < 0.001$). Moreover, the longitudinal analysis, performed in 98 patients, showed a significant enlargement of macular lesion area at an estimated exponential rate of 4.6% per year ($P = 0.046$), together with a significant worsening of BCVA (0.06 logMAR per year; $P < 0.001$) and a significant decrease of macular thickness (1.6% per year; $P = 0.005$) over the follow-up.

Conclusions. The current study describes, for the first time in literature, a longitudinal analysis of the macular lesion area assessed by SD-OCT in STGD1 disease, showing a significant progression over the follow-up. Our findings suggest that the evaluation of macular lesion area by en face SD-OCT, together with FAF, could drive the choice of the most amenable candidates and the most suitable area to be treated in gene therapy clinical trials.

Keywords: Stargardt disease, en face optical coherence tomography, fundus autofluorescence

Recessive Stargardt disease (STGD1) is the most common form of inherited macular dystrophy and is caused by mutations in the photoreceptor specific ATP binding cassette transporter (*ABCA4*) gene.[1] It is characterized by reduced central vision and atrophic-appearing foveal lesions, with or without yellowish-white fundus flecks at the posterior pole and/or midperipheral retina, primarily at the level of the retinal pigment epithelium (RPE).[2] To date, clinical diagnosis of STGD1 is based on various examinations: visual acuity, fundus exam, electroretinography (ERG), fundus autofluorescence (FAF) imaging, and fluorescein angiography.[2–4]

A recent additional exam is the spectral-domain optical coherence tomography (SD-OCT) that could provide specific clinical information useful for the follow-up of STGD1 patients.[5] Several studies analyzed the different morphologic aspects of macular changes in STGD1, including central retinal atrophy, disorganization and loss of inner and outer segment (IS/OS) junction (also known as ellipsoid zone; EZ),[5] thickening of external limiting membrane,[6] thickening of inner nuclear layer associated with outer nuclear layer thinning,[7] atrophic-appearing RPE complex,[8] extensive and severe thinning of the outer segment-plus layer (i.e., from the distal border of the RPE to the EZ band).[9] These studies focused on the B-scan cross-sectional images of SD-OCT, whereas the three-dimensional SD-OCT data set can be used to create an en face SD-OCT fundus image, by considering the relative values of each A-scan signal. Recently, a novel algorithm of advanced RPE analysis, known as the sub-RPE slab, has been introduced to create an en face image using only the light penetrating below the RPE into the choroid and sclera.[10]

The purpose of this study was to assess the disease progression in STGD1 patients in terms of morphologic changes assessed by SD-OCT. These findings may be useful for the clinical and surgical management of patients to be treated in future clinical trials; for example, for evaluation of gene therapy.

Materials and Methods

Study Design

The medical records of all 318 STGD1 patients, diagnosed at the Referral Center for Inherited Retinal Diseases of the Second

University of Naples from January 2009 to January 2012, were reviewed. The patients were screened for mutations in all 50 exons of the *ABCA4* gene as described previously.[5] Patients with a clinical and molecular diagnosis of Stargardt disease (at least one *ABCA4*-related mutation) and at least one yearly follow-up examination were included.

All patients included in the study underwent a complete ophthalmologic examination including best-corrected visual acuity (BCVA) by Snellen visual chart, slit-lamp biomicroscopy of the anterior segment and fundus examination, full-field ERG, and SD-OCT. Since outpatient service for FAF imaging was not working for a long time at our University Hospital, we considered FAF imaging only when available at the same visit as SD-OCT for comparison purposes.

The age of disease onset was defined as the age of initial symptoms, preferably confirmed by a documented medical record of macular dystrophy diagnosis (with or without BCVA reduction). The duration of the disease was computed as the difference between the age at our initial examination (study baseline) and the age of onset.

Fundus lesions were classified according to Fishman et al.[11] as follows: phenotype I) small atrophic-appearing foveal lesions and localized perifoveal yellowish-white flecks; phenotype II) numerous yellowish-white fundus lesions throughout the posterior pole; phenotype III) extensive atrophic-appearing RPE changes.

Full-field ERG was recorded by corneal contact lens electrodes with a Ganzfeld stimulator (EREV 2000 Electrophysiology system; LACE Elettronica, Pisa, Italy) according to the standards of the International Society for Clinical Electrophysiology of Vision (ISCEV).[12] Electroretinography abnormalities were classified according to Lois et al.[13]: group I) normal full-field amplitudes; group II) normal scotopic but reduced photopic b-wave amplitudes; group III) abnormal scotopic and photopic b-wave amplitudes.

Spectral-domain OCT (Cirrus HD-OCT; Carl Zeiss, Dublin, CA, USA) was performed according to the following protocol: the acquisition protocol comprised a five-line raster scan and a macular cube scan pattern (512×128 pixels) in which a 6×6-mm region of the retina was scanned within a scan time of 2.4 seconds. The retinal thickness analysis protocol provided with the instrument software was used to calculate the macular thickness. Moreover, the SD-OCT en face fundus image and the sub-RPE slab were obtained for each examination using the commercially available software on the Cirrus HD-OCT (version 6.0). The conventional SD-OCT fundus imaging is created by summing all pixel intensity values along individual A-scans, while the sub-RPE slab is an en face visualization using only the light penetrating below the RPE into the choroid and sclera. In the healthy regions of RPE, the pigment in the RPE will block most of the light penetrating into the choroid, while in areas of lesion, the underlying choroid will be illuminated.[10] The sub-RPE slab visualizations then were used to measure the area of RPE lesion by a proprietary completely automatic algorithm included in the Cirrus HD-OCT software.[14] Details about the automated algorithm have been reported previously.[10,14,15] Moreover, we computed the average diameter of RPE lesion area, assuming that the area is circular, and we determined the transverse extent of IS/OS junction loss in the foveal B-scan, with the measurement software from the SD-OCT machine, as suggested by Gomes et al.[16] Finally, we classified STGD1 patients into three categories based on the morphology of the IS/OS junction: (I) IS/OS junction preserved in the fovea, (II) IS/OS junction loss in the foveal area, and (III) extensive loss of IS/OS junction.[5]

Fundus autofluorescence images were obtained using a confocal scanning laser ophthalmoscope (Heidelberg Retina Angiograph [HRA]; Heidelberg Engineering, Heidelberg, Germany). The 30° field-of-view images were recorded after pupillary dilation. Standard procedure was followed for the acquisition of short-wavelength FAF images, including focus of the retinal image. An argon laser light (488 nm) was used for illumination, and a wide-band pass filter with cut-off at 500 nm was present in front of the detector. A series of nine FAF images $30° \times 30°$ encompassing the entire macular area with at least a portion of the optic disc, were recorded, digitalized, aligned for eye movements, and averaged to produce a single frame with improved signal-to-noise ratio. The area of absence of macular autofluorescence, which will be referred to as FAF lesion area, was measured using the measuring tool of the HRA software.

The study adhered to the tenets of the Declaration of Helsinki and received approval by the Local Ethics Committee. Moreover, each patient gave written informed consent.

Statistics

Our set of data is described by continuous (e.g., BCVA, age) and categorical (e.g., Fishman phenotype, Lois group, and so forth) variables. Continuous variables are expressed as mean (standard error of mean [SEM]; range), while categorical variables are reported as count (frequency). Only for the statistical regression analysis, BCVA was converted in logMAR. Repeated measure regression models were adopted to analyze the change of the clinical variables over follow-up time and the relationship between them. Models based on nontransformed and log-transformed values were fitted to estimate the linear and exponential annual rate of progression, respectively. All the regression models were estimated using Generalized Estimating Equations, which enable to include correlated data, such as the value from both eyes of the same patients, and repeated measurements over time (longitudinal data), by adopting an appropriate covariance structure, as described previously.[17] A P value less than 5% was considered statistically significant.

Results

The study cohort consisted of 318 patients with a clinical diagnosis of STGD1 who initially were identified for possible inclusion in the study. Among them, we excluded 220 patients for the following reasons: no mutation in *ABCA4* (41 patients), and incomplete or no follow-up data (179 patients).

We selected 98 STGD1 patients, with a mean age of 30 years (SEM, 1.4 years; range, 9–60 years), and a mean disease duration of 13 years (SEM, 1 year; range, 0–47 years). Mean BCVA, evaluated in all patients, was 20/100 (SEM, 20/1000; range, 20/2400–20/20) for both eyes. Ophthalmoscopic lesions were consistent with Fishman phenotype I in 55 patients (56.2%), Fishman phenotype II in 26 (26.5%), and Fishman phenotype III in 17 (17.3%). Electroretinographic responses were consistent with Lois group I in 58 patients (59.1%), Lois group II in 8 (8.2%), and Lois group III in 32 (32.7%).

The mean RPE lesion area, measured by SD-OCT, was 3.26 mm^2 (SEM, 0.43 mm^2; range, 0–17.8 mm^2) in right eyes, and 3.06 mm^2 (SEM, 0.39 mm^2; range, 0–17.0 mm^2) in left eyes. Figures 1 and 2 show the mean RPE lesion area assessed by en face SD-OCT in a patient with foveal involvement and in one with foveal sparing, respectively.

Age and duration of disease were significant predictors of RPE lesion area over time, but age offered a significantly better fit of the data compared to duration of disease. In particular, a significant enlargement of 3.5% per year of age (95% confidence interval [CI], 2.9%–4.1%; $P < 0.001$) was estimated by baseline values in both eyes, as represented by the exponential regression model shown in Figure 3.

Investigative Ophthalmology & Visual Science

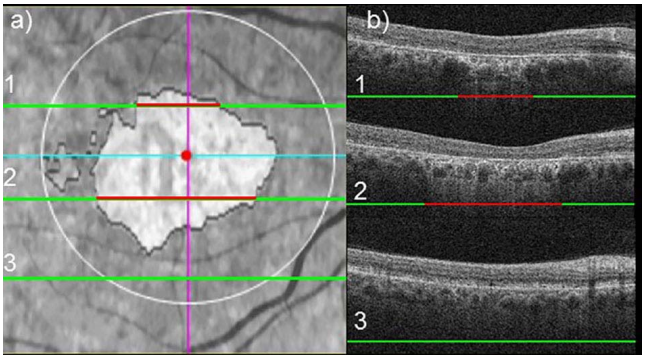

Figure 1. Example of en face SD-OCT in a STGD1 patient with foveal involvement. En face SD-OCT fundus image (**a**). Three OCT B-scans are reported to show the extent of RPE lesion area (**b**): *red lines* indicate segments affected by RPE lesion, whereas *green lines* indicate segments not affected by RPE lesion.

The RPE lesion area was significantly higher in the Fishman III compared to Fishman I ($\beta = 4.68$, $P < 0.001$), Lois III compared to Lois I ($\beta = 3.54$, $P < 0.001$), IS/OS III compared to IS/OS I ($\beta = 5.57$, $P < 0.001$), and IS/OS II compared to IS/OS I ($\beta = 1.16$; $P < 0.001$) groups. Furthermore, RPE lesion area correlated significantly with BCVA ($\beta = 0.97$, $P < 0.045$) and macular thickness ($\beta = 0.016$, $P = 0.008$). Finally, the diameter of RPE lesion area significantly correlated with the transverse extent of IS/OS junction loss in the fovea ($\beta = 0.56$, $P < 0.001$) and is significantly smaller than the IS/OS junction loss ($P < 0.001$).

To evaluate the correlation between RPE lesion area by SD-OCT and macular atrophy determined by FAF imaging, we compared the two measurements in the subgroup of 22 patients (15 females and 7 males; aged 37.1 ± 2.8 years, range, 16–71 years). The mean disease duration was 13.6 years (SEM, 2.2 years). Mean BCVA was 20/200 (SEM, 20/1000; range, 20/2400–20/20) for both eyes. Ophthalmoscopic lesions were consistent with Fishman phenotype I in 12 patients (54.5%), Fishman phenotype II in 4 (18.2%), and Fishman phenotype III in 6 (27.3%). Electroretinographic responses were consistent with Lois group I in 17 patients (77.3%), Lois group II in 2 (9.0%), and Lois group III in 3 (13.6%). We observed a mean absent FAF area of 5.0 mm^2 (SEM, 1.2 mm^2) and 4.9 mm^2 (SEM, 0.9 mm^2) in right and left eyes, respectively. From en face SD-OCT scans mean RPE lesion areas of 4.4 mm^2 (SEM, 0.9 mm^2) and 4.4 mm^2 (SEM, 0.8 mm^2) were estimated in right and left eyes, respectively. The linear regression model fitted to compare the extent of RPE lesion area with the absent FAF area indicates a significant correlation between the two parameters ($\beta = 0.82$; Standard Error = 0.03; 95% CI = 0.76–0.88; $R^2 = 0.94$; $P < 0.001$).

These 98 patients were followed for a median of 3 years (minimum follow-up 1 year; maximum 5 years). The values of RPE lesion area of each patient were compared over the follow-up time points and Figure 4 shows the comparison of two en face fundus SD-OCT images (i.e., at baseline and at the last follow-up visit) in a selected patient, with a marked enlargement of RPE lesion area. The longitudinal data analysis revealed a significant enlargement of RPE lesion area at an estimated linear rate of 0.160 mm^2/year (95% CI, 0.018–0.303, $P = 0.027$) and a mean exponential rate of 4.6%/year (95% CI, 0.1%–9.9%, $P = 0.046$). Moreover, we observed a significant thinning of macular thickness at an estimated linear rate of −2.03 μm/year (95% CI, −3.45 to 0.616, $P = 0.005$) and a mean exponential rate of −1.6%/year (95% CI, −2.6% to −0.5%, $P = 0.005$). Finally, the BCVA significantly worsened at an estimated rate of 0.060 logMar/year (95% CI, 0.038–0.082, $P < 0.001$), corresponding to 3 Early Treatment of Diabetic Retinoscopy Study (ETDRS) letters per year.

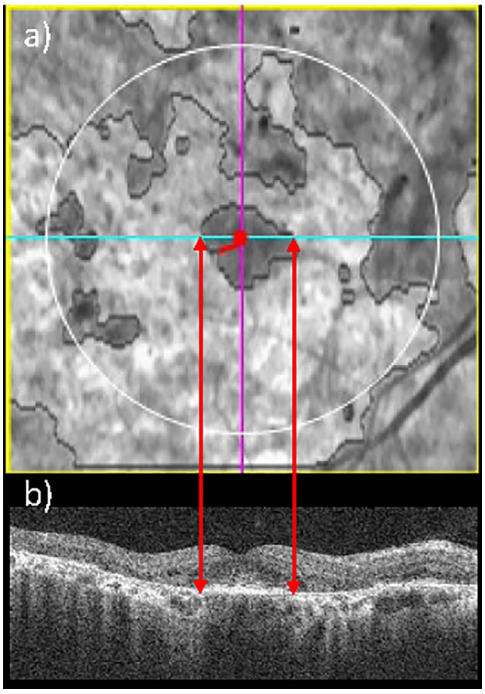

Figure 2. Example of en face SD-OCT, which enables to identify a STGD1 patient with foveal sparing. En face SD-OCT fundus image (**a**): the *red dot* represents the fovea (automatically detected) and the *light blue line* indicates the corresponding B-scan. Spectral-domain OCT B-scan corresponding to the fovea (**b**) highlights that the fovea is not affected by RPE lesion.

Discussion

The present study investigates a large cohort of STGD1 patients with a multiyear follow-up (up to 5 years), focusing on morphologic changes evaluated by SD-OCT, in particular, RPE lesion area.

On the basis of previous studies,[18–20] disease-linked mutations in ABCA4 protein lead to alterations in RPE and photoreceptor layers. Although the exact sequence of events in the development of photoreceptor and RPE atrophy in STGD1 remains controversial, the most accepted hypothesis is that atrophy of the RPE occurs initially, with secondary photoreceptor degeneration.[21] For that reason, quantification of RPE atrophy by morphologic imaging was adopted to evaluate the disease progression[22–24] and could be useful to assess the therapeutic effect of experimental treatment. In particular, in the current study, we adopted a fully automatic algorithm, recently developed by Gregori et al.,[15] available on the Cirrus HD-OCT. The three dimensional OCT data set is used to create an en face SD-OCT fundus image, which enables the visualization of atrophy as a bright area due to the increased penetration of light into the choroid where atrophy has occurred. The increased SD-OCT signal associated with atrophy arises from the absence of the RPE and choriocapillaris, which are the two layers of the eye that normally cause the incident light to scatter, thus, preventing deeper transmission of light into the choroid.[25] The algorithm identifies and measures areas of sub-RPE illumination where SD-OCT signal is able to penetrate through the choroid, indicating that the RPE is atrophic (Figs. 1, 2). The reproducibility of the automated

Investigative Ophthalmology & Visual Science

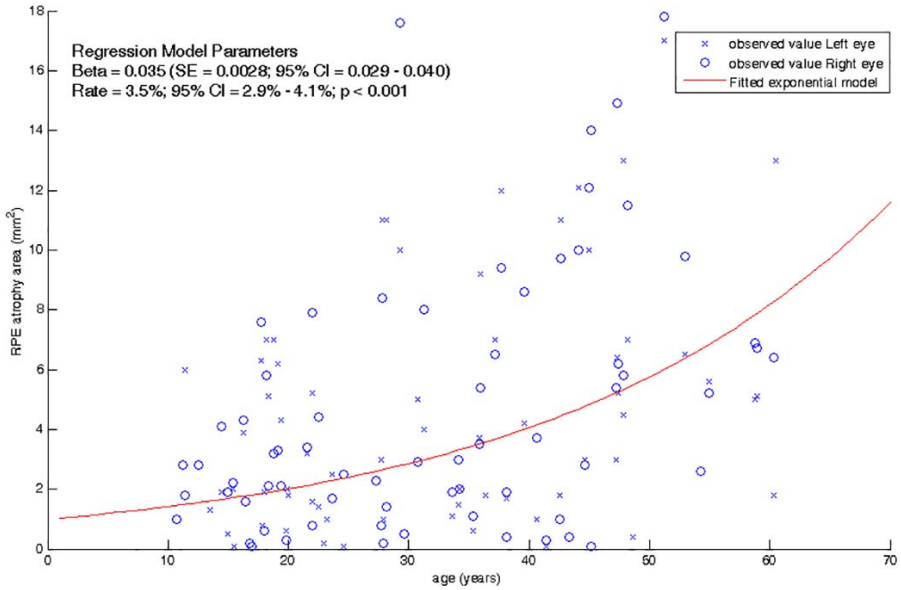

Figure 3. Macular RPE atrophy area in function of age in STGD1 patients. *Red continuous line* represents the exponential model fitted with repeated measurement regression by Generalized Estimating Equation.

measurements also was assessed in our STGD1 cohort by computing the intraclass correlation coefficient (ICC) between SD-OCT scans performed within 1 week in 15 patients and was excellent (ICC = 0.994; 95% CI, 0.982–0.998).[26] Finally, since FAF was commonly adopted in STGD1 to assess macular atrophy area,[9,21,27] we compared the RPE lesion area measurements by SD-OCT to the FAF lesion area in the subset of STGD1 patients who underwent both examinations during the same visit. Since most patients underwent only SD-OCT and not FAF examination, only a relatively small number of cases (n = 22) could be included in the comparison between the two techniques. We believe that this sampling, due to technical reasons, should not introduce a selection bias, also as no statistical difference was observed between the subset of 22 patients and the overall sample in terms of disease length, BCVA, distribution according to Fishman and Lois classifications ($P > 0.10$) Moreover, the sample size is sufficient to observe a significant and strong correlation (type 1 error probability, 0.05; statistical power > 0.90; expected slope of linear regression line, 0.8) between the two measurements, showing the reliability of the automatic SD-OCT algorithm in STGD1.

Using the automated algorithm on en face SD-OCT image, we observed that the RPE lesion area was significantly larger in the more severe STGD1 phenotype groups, such as Fishman III, Lois III, IS/OS III and II groups. Moreover, it correlated significantly with BCVA and mean macular thickness values; the average diameter, computed by RPE lesion area, significantly correlated with the transverse extent of IS/OS junction loss in the foveal scan and is smaller than IS/OS loss. To this regard, our results are consistent with the findings by Gomes et al.[16] who showed, by SD-OCT scans, that the underlying band of the RPE complex is relatively preserved compared to the photoreceptor layer in STDG1 patients.

Finally, the rate of disease progression of RPE lesion area was assessed over a multiyear follow-up: in particular, we observed an increase of RPE lesion area at an estimated linear rate of 0.16 mm²/year (range, 0–4.75 mm²/year). This value was comparable with the mean rate of atrophy enlargement computed by FAF and reported in longitudinal studies: Fujinami et al.[22] (0.45 mm²/year; range, 0.00–5.89 mm²/year); Mcbain et al.[23] (1.58 mm²/year; SD, 1.25 mm²/year; range, 0.13–5.27 mm²/year), and Chen et al.[24] (0.94 mm²/year; SD, 0.87 mm²/year; range, 0.2–2.13 mm²/year).

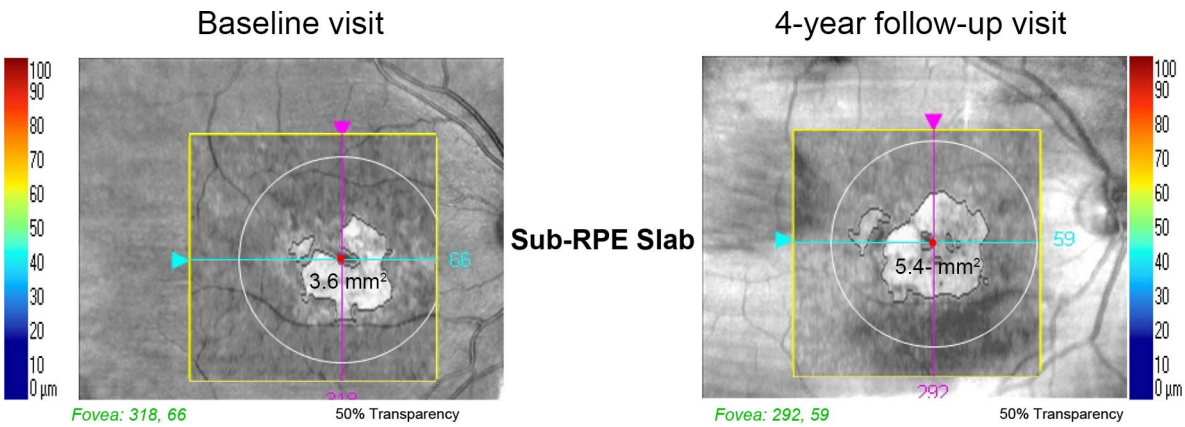

Figure 4. Comparison of en face fundus SD-OCT images in a STGD1 patient between two visits. The macular RPE atrophy changed from 3.6 to 5.4 mm², over a 4-year follow-up, corresponding to an enlargement of about 0.45 mm² per year (about 10.7% per year).

Investigative Ophthalmology & Visual Science

Although FAF is widely used in research studies, some limits of the techniques have been shown, for example, the difficulty in obtaining measurements from discrete areas of atrophy in presence of eye movements (i.e., in instable fixation).[28] Moreover, some advantages of the SD-OCT technique compared to FAF have been highlighted by recent studies: Sayegh et al.[29] showed that, thanks to the easy and automatic detection of foveal depression by SD-OCT, foveal sparing can be identified by SD-OCT with a higher certainty and intergrader agreement than with FAF; Gomes et al.[16] suggested that SD-OCT could be more sensitive in detecting small lesion areas, showing that the diameter of the area of central atrophy identified by the absence of FAF underestimates the extent of the transverse loss of the IS/OS junction (indicating photoreceptor atrophy), assessed by SD-OCT. However, the automated SD-OCT algorithm based on sub-RPE slab, adopted in the current study, has been shown to underestimate the size of larger lesions in patients with age-related macular degeneration.[30] Our data seem to confirm this limit of the automated algorithm also in STGD1 patients. As suggested by Yehoshua et al.,[30] this difference may be the result of the degenerating RPE along the border of the atrophy: the amount of light at the borders may vary depending on the amount of melanin present and the integrity of the choriocapillaris; as a result, the algorithm may miss some parts of the lesion with irregular brightness and/or poor contrast. This limit of the algorithm has been addressed by the manufacturer providing an editor tool for manually modifying the boundaries of the lesion area. In the current study, we did not use this functionality, since we aimed at evaluating the completely automated algorithm. Finally, another reason of underestimation could be due to the fact that the automatic SD-OCT algorithm selected only the macular area (circular area of 2.5 mm of radius).

Currently, the de facto gold standard to measure RPE atrophy in STGD1 and other macular degenerations (e.g., age-related macular degeneration) is FAF imaging. Our findings pave the way to the adoption of en face SD-OCT through a completely automated algorithm for quantitatively assessing RPE atrophy in STGD1 as a complementary test to FAF imaging. For instance, a combined outcome based on SD-OCT and FAF could be adopted to measure treatment efficacy in STGD1 clinical trials. Moreover, the evaluation of RPE lesion area assessed by SD-OCT could be adopted to choose the best area to be treated (i.e., an area in proximity to fovea but partially or not affected by RPE atrophy), particularly, with the introduction of intraoperative SD-OCT which could enable the control of the treatment area.[31] Finally, SD-OCT offers a better definition of retinal alterations by cross-sectional scans, which enable the visualization of RPE and photoreceptor layers.

The current study presents some limits, mainly related to its retrospective design: only short-wavelength FAF images (not near-infrared) were available, the comparison with FAF imaging was possible only in a small subgroup of patients, and the absence of follow-up data caused the exclusion of a large number of patients. Further prospective studies designed to compare the two techniques are needed to confirm the SD-OCT as gold standard method for morphologic evaluation of disease progression in STDG1.

Our study shows that en face SD-OCT, particularly, sub-RPE slab visualization, could be adopted to evaluate disease progression in STGD1 patients. The longitudinal analysis showed an enlargement of the RPE atrophy area, together with a significant worsening of BCVA and a thinning of macular thickness over the follow-up in the majority of patients. In addition, SD-OCT provides en face and cross-sectional images of the macula. Finally, since gene therapy strategies for *ABCA4*-related retinal degenerations are under investigation in preclinical studies and in humans, morphologic measurements of disease progression, such as RPE lesion area, could drive the choice of the most amenable candidates and the most suitable area to be treated in future clinical trials.

Acknowledgments

The authors thank Carmela Acerra for text editing, Emanuele Monteasi and Carlo Perillo (ophthalmic technicians) for the performance of some examinations.

Supported by Grant "Therapeutic approaches for ABCA4-associated disorders" (1R24EY019861-01A1) from the National Eye Institute.

Disclosure: **P. Melillo**, Sanofi R&D (C); **F. Testa**, Sanofi R&D (C); **S. Rossi**, None; **V. Di Iorio**, None; **A. Orrico**, None; **A. Auricchio**, None; **F. Simonelli**, Sanofi R&D (C)

References

1. Allikmets R, Singh N, Sun H, et al. A photoreceptor cell-specific ATP-binding transporter gene (ABCR) is mutated in recessive Stargardt macular dystrophy. *Nat Genet*. 1997;15:236–246.
2. Stargardt K. Über familiäre, progressive Degeneration in der Maculagegend des Auges. *Graefes Arch Clin Exp Ophthalmol*. 1909;71:534–550.
3. Armstrong JD, Meyer D, Xu S, Elfervig JL. Long-term follow-up of Stargardt's disease and fundus flavimaculatus. *Ophthalmology*. 1998;105:448–457; discussion 457–448.
4. Rotenstreich Y, Fishman GA, Anderson RJ. Visual acuity loss and clinical observations in a large series of patients with Stargardt disease. *Ophthalmology*. 2003;110:1151–1158.
5. Testa F, Rossi S, Sodi A, et al. Correlation between photoreceptor layer integrity and visual function in patients with Stargardt disease: implications for gene therapy. *Invest Ophthalmol Vis Sci*. 2012;53:4409–4415.
6. Lee W, Noupuu K, Oll M, et al. The external limiting membrane in early-onset Stargardt disease. *Invest Ophthalmol Vis Sci*. 2014;55:6139–6149.
7. Huang WC, Cideciyan AV, Roman AJ, et al. Inner and outer retinal changes in retinal degenerations associated with ABCA4 mutations. *Invest Ophthalmol Vis Sci*. 2014;55:1810–1822.
8. Park JC, Collison FT, Fishman GA, et al. Objective analysis of hyperreflective outer retinal bands imaged by optical coherence tomography in patients with Stargardt disease. *Invest Ophthalmol Vis Sci*. 2015;56:4662–4667.
9. Greenstein VC, Schuman AD, Lee W, et al. Near-infrared autofluorescence: its relationship to short-wavelength autofluorescence and optical coherence tomography in recessive stargardt disease. *Invest Ophthalmol Vis Sci*. 2015;56:3226–3234.
10. Yehoshua Z, Rosenfeld PJ, Gregori G, et al. Progression of geographic atrophy in age-related macular degeneration imaged with spectral domain optical coherence tomography. *Ophthalmology*. 2011;118:679–686.
11. Fishman GA, Farber M, Patel BS, Derlacki DJ. Visual acuity loss in patients with Stargardt's macular dystrophy. *Ophthalmology*. 1987;94:809–814.
12. Marmor MF, Fulton AB, Holder GE, Miyake Y, Brigell M, Bach M. ISCEV standard for full-field clinical electroretinography (2008 update). *Doc Ophthalmol*. 2009;118:69–77.

13. Lois N, Holder GE, Bunce C, Fitzke FW, Bird AC. Phenotypic subtypes of Stargardt macular dystrophy-fundus flavimaculatus. *Arch Ophthalmol*. 2001;119:359–369.
14. Ahlers C, Gotzinger E, Pircher M, et al. Imaging of the retinal pigment epithelium in age-related macular degeneration using polarization-sensitive optical coherence tomography. *Invest Ophthalmol Vis Sci*. 2010;51:2149–2157.
15. Gregori G, Wang F, Rosenfeld PJ, et al. Spectral domain optical coherence tomography imaging of drusen in nonexudative age-related macular degeneration. *Ophthalmology*. 2011;118: 1373–1379.
16. Gomes NL, Greenstein VC, Carlson JN, et al. A comparison of fundus autofluorescence and retinal structure in patients with Stargardt disease. *Invest Ophthalmol Vis Sci*. 2009;50:3953–3959.
17. Testa F, Melillo P, Di Iorio V, et al. Macular function and morphologic features in juvenile Stargardt disease: longitudinal study. *Ophthalmology*. 2014;121:2399–2405.
18. Sparrow JR, Nakanishi K, Parish CA. The lipofuscin fluorophore A2E mediates blue light–induced damage to retinal pigmented epithelial cells. *Invest Ophthalmol Vis Sci*. 2000; 41:1981–1989.
19. Sparrow JR, Boulton M. RPE lipofuscin and its role in retinal pathobiology. *Exp Eye Res*. 2005;80:595–606.
20. Molday RS. ATP-binding cassette transporter ABCA4: molecular properties and role in vision and macular degeneration. *J Bioenerg Biomembr*. 2007;39:507–517.
21. Ritter M, Zotter S, Schmidt WM, et al. Characterization of Stargardt disease using polarization-sensitive optical coherence tomography and fundus autofluorescence imaging. *Invest Ophthalmol Vis Sci*. 2013;54:6416–6425.
22. Fujinami K, Lois N, Mukherjee R, et al. A longitudinal study of Stargardt disease: quantitative assessment of fundus autofluorescence, progression, and genotype correlations. *Invest Ophthalmol Vis Sci*. 2013;54:8181–8190.
23. McBain VA, Townend J, Lois N. Progression of retinal pigment epithelial atrophy in stargardt disease. *Am J Ophthalmol*. 2012;154:146–154.
24. Chen B, Tosha C, Gorin MB, Nusinowitz S. Analysis of autofluorescent retinal images and measurement of atrophic lesion growth in Stargardt disease. *Exp Eye Res*. 2010;91:143–152.
25. Chen Q, de Sisternes L, Leng T, Zheng L, Kutzscher L, Rubin DL. Semi-automatic geographic atrophy segmentation for SD-OCT images. *Biomed Opt Express*. 2013;4:2729–2750.
26. Melillo P, Rossi S, Di Iorio V, et al. Reproducibility of en-face optical coherence tomography imaging for macular atrophy area evaluation in juvenile macular degeneration. In: *XIV Mediterranean Conference on Medical and Biological Engineering and Computing 2016*. Cham: Springer International Publishing; 2016:250–253.
27. Sparrow JR, Marsiglia M, Allikmets R, et al. Flecks in recessive Stargardt disease: short-wavelength autofluorescence, near-infrared autofluorescence, and optical coherence tomography. *Invest Ophthalmol Vis Sci*. 2015;56:5029–5039.
28. Duncker T, Tsang SH, Lee W, et al. Quantitative fundus autofluorescence distinguishes ABCA4-associated and non-ABCA4-associated bull's-eye maculopathy. *Ophthalmology*. 2015;122:345–355.
29. Sayegh RG, Simader C, Scheschy U, et al. A systematic comparison of spectral-domain optical coherence tomography and fundus autofluorescence in patients with geographic atrophy. *Ophthalmology*. 2011;118:1844–1851.
30. Yehoshua Z, Garcia Filho CA, Penha FM, et al. Comparison of geographic atrophy measurements from the OCT fundus image and the sub-RPE slab image. *Ophthalmic Surg Lasers Imaging Retina*. 2013;44:127–132.
31. Falkner-Radler CI, Glittenberg C, Hagen S, Benesch T, Binder S. Spectral-domain optical coherence tomography for monitoring epiretinal membrane surgery. *Ophthalmology*. 2010;117:798–805.

Investigative Ophthalmology & Visual Science